Ultratransparent Media and Transformation Optics with Shifted Spatial Dispersions

Jie Luo,[1] Yuting Yang,[1] Zhongqi Yao,[1] Weixin Lu,[1] Bo Hou,[1] Zhi Hong Hang,[1,*] C. T. Chan,[2] and Yun Lai[1,†]

[1]*College of Physics, Optoelectronics and Energy & Collaborative Innovation Center of Suzhou Nano Science and Technology,
Soochow University, Suzhou 215006, China*
[2]*Department of physics and Institute for Advanced Study, Hong Kong University of Science and Technology,
Clear Water Bay, Hong Kong*

By using pure dielectric photonic crystals, we demonstrate the realization of ultratransparent media, which allow near 100% transmission of light for all incident angles and create aberration-free virtual images. The ultratransparency effect is well explained by spatially dispersive effective medium theory for photonic crystals, and verified by both simulations and proof-of-principle microwave experiments. Designed with shifted elliptical equal frequency contours, such ultratransparent media not only provide a low-loss and feasible platform for transformation optics devices at optical frequencies, but also enable new freedom for phase manipulation beyond the local medium framework.

Transparent media are the foundation of almost all optical systems. However, due to general reflection caused by impedance mismatch [Fig. 1(a)], transparency has never been perfect in natural materials such as dielectrics. In the past decades, artificial electromagnetic materials like photonic crystals (PhCs) [1–18] and metamaterials [19–22] have been proposed to realize unusual electromagnetic properties beyond natural materials. Research on PhCs was mostly focused on photonic band gaps that block waves [Fig. 1(b)]. The theory of transformation optics (TO) [17,18,23–44], however, shows that metamaterials in principle can realize perfectly transparent media, which exhibit the rare property of omnidirectional impedance matching and thus eliminate all reflections. Such perfect transparency is also one of the critical requirements in novel TO devices such as invisibility cloaks [23–37], concentrators [38], illusion optics devices [39,40], simulations of cosmic phenomena [42–44], etc. However, in practice, there exists great difficulty in realizing such perfect transparency by metamaterials. In fact, most previous TO experiments were realized by using the so-called "reduced parameters," which maintain the refractive behavior, but sacrifice the impedance matching as well as the perfect transparency [25,26,28–31]. Such an approximation leads to general reflection [Fig. 1(c)]. At optical frequencies, the inherent loss in metallic components of metamaterials makes the realization of perfect transparency as well as the ideal nonreflecting TO devices extremely difficult [45,46], if not impossible.

In this work, we propose to utilize the spatial dispersive effective parameters of pure dielectric PhCs to realize perfectly transparent media with omnidirectional impedance matching, which allows near 100% transmission of light at all incident angles. The equal frequency contours (EFCs) of such PhCs are designed to be elliptical and

shifted in k space, and thus contain strong spatial dispersions. We demonstrate that at certain frequency regimes, such PhCs can allow the maximal amount of light to pass through and create aberration-free virtual images. Therefore, they are superior to normal transparent media like dielectrics, and hereby denoted as ultratransparent media. Interestingly, the combination of perfect transparency and elliptical EFCs satisfies the essential requirement of ideal TO devices. Such PhCs provide a low-loss and feasible platform for TO devices at optical frequencies. The shift of EFC also enables new freedom for phase manipulation beyond the local medium framework. The ultratransparency effect of PhCs and its application in TO have been verified by numerical simulations and proof-of-principle microwave experiments.

Without loss of generality, we consider transverse electric (TE, with electric field in the z direction) polarized light incident onto a slab of a spatially dispersive medium in the xy plane. For reasons to be explained below, we let the ultratransparent medium exhibit the following special EFCs:

$$\frac{(k_x - p)^2}{q} + k_y^2 = k_0^2, \tag{1}$$

where k_0 is the wave number in air, $k_{x(y)}$ is the $x(y)$ component of the wave vector, p denotes the displacement from the Brillouin zone center, and q determines the ratio of the k_y and k_x axes of the ellipse, as shown in the inset graphs of Fig. 1(d). Note that such an EFC is of the same height, i.e., the maximum $|k_y|$, with the EFC of free space.

We have chosen such shifted EFCs because of the following reasons. First, it has been previously pointed out that media with EFCs of elliptical shapes can be used to create TO devices [17]. Controllable elliptical EFCs are the
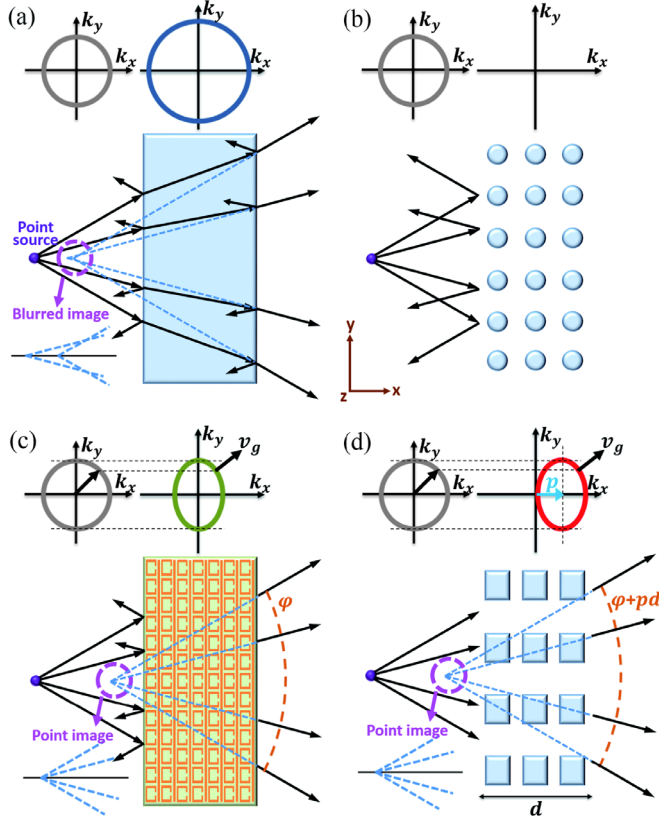
FIG. 1. (a) Virtual image formation through a dielectric slab, with general reflection and aberration. (b) Total reflection by a PhC slab with complete photonic band gap. (c) Virtual image formation through a metamaterial slab, without aberrations, but with reflection. (d) Aberration-free virtual image formation through an ultratransparent PhC without any reflection due to omnidirectional impedance matching. The black arrows and blue dashed lines in (a)–(d) represent the light rays from a point source, and the back tracing lines, respectively. The yellow dashed curves in (c) and (d) indicate equal phase surfaces of transmitted rays, with different phases φ and $\varphi + pd$, respectively. The inset graphs show the corresponding EFCs.

essential reason for the controllable refractive behaviors in many TO applications. In this case, although the EFC is shifted away from the Brillouin zone center, the refractive behavior for light incident on the surface perpendicular to the shift direction is, however, completely retained, as shown in Fig. 1(d). Moreover, hereby we prove that elliptical EFCs also enable the formation of aberration-free virtual images. By using ray optics, it can be easily shown that transmitted rays from a point source behind a dielectric slab would form a "blurred" area of virtual image rather than a point image [shown in Fig. 1(a)], which is induced by the mismatch between the EFCs of free space and dielectrics. However, for a metamaterial slab exhibiting an elliptical EFC [as shown in Fig. 1(c)], an ideal point image would be formed. This actually can be understood as a direct consequence of TO. Since the shift of EFCs does not change the refractive behavior at all, aberration-free

virtual images can also be formed by a slab of medium with a shifted EFC described by Eq. (1) for waves incident onto the interface perpendicular to this shifting direction [shown in Figs. 1(d)]. An analytical proof by both ray optics and wave optics is described in the Supplemental Material [47], Sec. II, demonstrating the absence of monochromatic aberrations [52,53]. We note that such an aberration-free virtual imaging behavior shows a fundamental difference between our system and normal dielectric media. In dielectric slabs, the image information is gradually smeared during the propagation of light. While in our system, the image information can be maintained, up to the diffraction limit.

Second, the shift of EFCs provides more possibilities for omnidirectional impedance matching. We assume that the medium can be characterized by relative permittivity tensor $\boldsymbol{\varepsilon}(k_y)$ and relative permeability tensor $\boldsymbol{\mu}(k_y)$ for certain angular frequency ω. Here we only consider propagating waves and, thus, k_x can be determined from the EFC which links k_x and k_y. The dispersion relation of propagating waves in the spatially dispersive medium can be expressed as $k_x^2/\mu_y(k_y) + k_y^2/\mu_x(k_y) = \varepsilon_z(k_y)k_0^2$. Here, we define the impedance of the spatially dispersive media as $Z \equiv E_z/H_y = -[\mu_0\mu_y(k_y)/k_x]\omega$ for TE polarization. By matching the wave impedance of the spatially dispersive medium with that of free space, i.e., $Z_0 = -(\mu_0/\sqrt{k_0^2 - k_y^2})\omega$ (See the Supplemental Material [47] Sec. I), we obtain

$$\frac{\mu_x(k_y)\mu_y(k_y)}{\mu_x(k_y)\varepsilon_z(k_y)k_0^2 - k_y^2} = \frac{1}{k_0^2 - k_y^2}. \qquad (2)$$

If Eq. (2) can be satisfied for all $|k_y| < k_0$, then omnidirectional impedance matching can be achieved, which leads to near 100% transmission of light for all incident angles.

An obvious local medium solution of Eq. (2) is that $\mu_x\mu_y = 1$ and $\mu_x\varepsilon_z = 1$, which corresponds to elliptical EFCs centered at the Brillouin zone center and is consistent with TO theory. However, this is not the only possible solution for spatially dispersive media. Now, we consider the medium with the EFC described by Eq. (1), i.e., $k_x = p \pm \sqrt{q(k_0^2 - k_y^2)}$. By substituting this relation into Eq. (2) and the spatial dispersion, we obtain the analytical forms of spatially dispersive parameters as $\mu_y^2(k_y) = [p \pm \sqrt{q(k_0^2 - k_y^2)}]^2/(k_0^2 - k_y^2)$ and $\varepsilon_z(k_y)k_0^2 - k_y^2/\mu_x(k_y) = \pm[p \pm \sqrt{q(k_0^2 - k_y^2)}]\sqrt{k_0^2 - k_y^2}$. The general solutions for omnidirectional impedance matching of spatially dispersive media are discussed in the Supplemental Material [47], Sec. I.

By combining the omnidirectional impedance matching and aberration-free virtual imaging, we obtain a type of

material that is significantly more transparent than normal dielectric solids. In this sense, we denote them as ultra-transparent media.

PhCs contain strong spatial dispersions and thus provide the perfect candidate for realization of ultratransparent media. First, we demonstrate a type of PhCs composed of a rectangular array of dielectric rods in free space, with the unit cell shown in Fig. 2(a). Under TE polarization, the band structure is presented in Fig. 2(b), and the EFC of the third band is plotted in the reduced first Brillouin zone in Fig. 2(c). At the working frequency $fa/c = 0.3183$, where c is the speed of light in free space and a is the unit length, the corresponding EFC is indeed a shifted ellipse that can be described by Eq. (1) with $p \approx \pi/a$. Figure 2(d) shows the impedance difference of the PhC and free space of the third band, i.e., $|(Z - Z_0)/(Z + Z_0)|$, showing very small difference for a very large range of k_y at the working
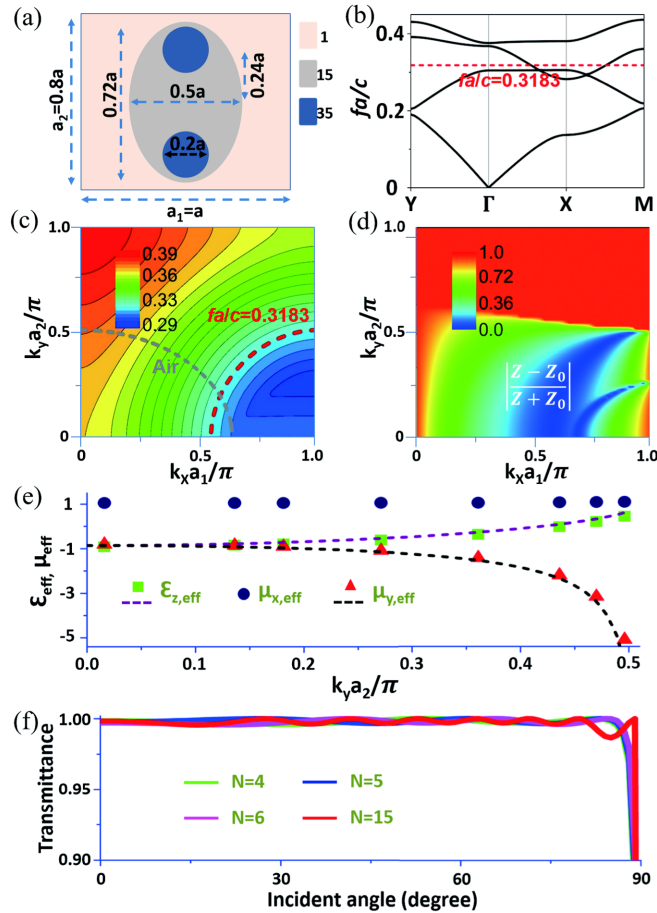

FIG. 2. (a) Illustration of the unit cell of the ultratransparent PhC. (b) The band structure of the PhC. (c) The EFC of the third band. (d) The impedance difference of the PhC and free space of the third band. (e) The effective parameters $\varepsilon_{z,\text{eff}}$, $\mu_{x,\text{eff}}$, and $\mu_{y,\text{eff}}$ retrieved from the eigenfields (symbols) and predicted by the ultratransparency conditions (dashed lines). (f) Calculated transmittance through a PhC slab with $N(= 4, 5, 6, 15)$ layers of unit cells as functions of the incident angle.

frequency. Then, by matching the dispersion and surface impedance of the eigenstates in the PhC with the propagating waves in a spatially dispersive medium, the k-dependent effective parameters can be obtained (see the Supplemental Material [47], Sec. III), which are denoted by dots in Fig. 2(e). Clearly, we find $\mu_{x,\text{eff}} \approx 1$, while $\varepsilon_{z,\text{eff}}$ and $\mu_{y,\text{eff}}$ are both dependent on k_y. We note that our method also provides a general approach to retrieve the k-dependent effective parameters of PhCs and metamaterials. At relatively low frequencies, this method shows a high validity and accuracy in describing the effective media of nonlocal systems. Moreover, the k dependence of $\varepsilon_{z,\text{eff}}$ and $\mu_{y,\text{eff}}$ coincides excellently with the requirement for omnidirectional impedance matching (dashed lines), which is previously obtained analytically. To verify the unique behavior, we have numerically calculated the transmittance through such a PhC slab consisting of $N(=4, 5, 6, 15)$ layers of unit cells in the x direction, as shown in Fig. 2(f). It is shown that the transmittance is near unity (>99%) for nearly all incident angles ($\theta_i < 89°$), and is almost irrespective of the layer number N, indicating that the ultra-transparency effect is a result of impedance matching instead of tunneling effects.

In the design process, we first find out the band exhibiting the shifted EFC in the band structure. The shift can be controlled by modifying the microstructure of PhCs. Then, we engineer the structure of PhC so as to ensure impedance matching of the eigenstates with propagating waves in free space, in an angle range as large as possible [54]. Nearly omnidirectional impedance matching can be gradually obtained after a trial-and-error iterative optimal algorithm.

For transparency in a relatively smaller range of incident angles, the design process is much easier and the effect can exist in much simpler structures. In the following, we demonstrate a simple ultratransparent PhC, which is verified by proof-of-principle microwave experiments. The PhC consists of rectangular alumina ($\varepsilon = 8.5$) bars in a square lattice and also exhibits a shifted elliptical EFC (see the Supplemental Material [47], Sec. VI). Numerical simulations show that the transmittance exceeds 99% for all incident angles of $\theta_i < 60°$ under TE polarization. A 23×5 array of such a PhC is assembled in the xy plane inside a parallel-plate waveguide composed of two flat aluminum plates, as shown in Fig. 3(a). The lattice constant is $a = 12$ mm and the size of each alumina bar is $4.8(w_2) \times 9.6(w_1) \times 10$ mm. The electric field was measured via an antenna fixed in a hole in the upper metal plate (not shown here). The measured electric fields for 45° incident angle at the working frequency of 11.8 GHz is shown in Fig. 3(b) with barely noticeable reflection. We note that the divergence of the transmitted beam is mainly caused by the intrinsic divergence of the Gaussian beam and imperfections of the experimental setup. In Fig. 3(c), the measured transmittance (triangular dots) coincides with simulation results (solid lines) quite well, both showing great
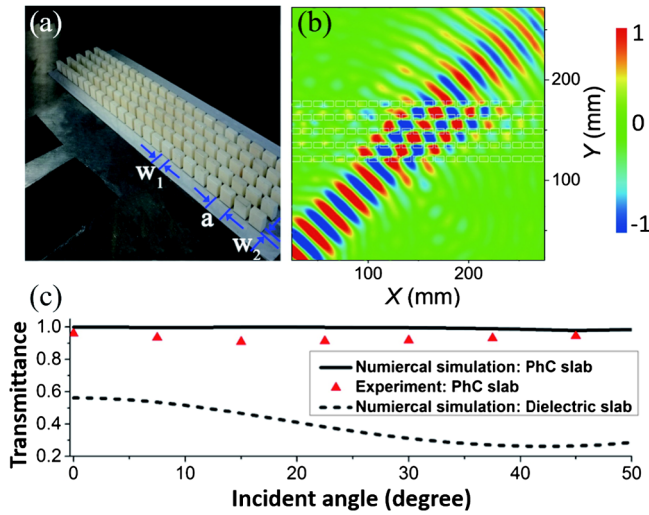
FIG. 3. (a) Photo of the PhC composed of alumina bars (white) placed inside the microwave field mapper. (b) The measured electric-field distributions for beams with incident angles of 45°. (c) Transmittance through the PhC slab in simulations (solid lines) and experiments (triangular dots) and an alumina slab having the same thickness (dashed lines) as the function of incident angles.
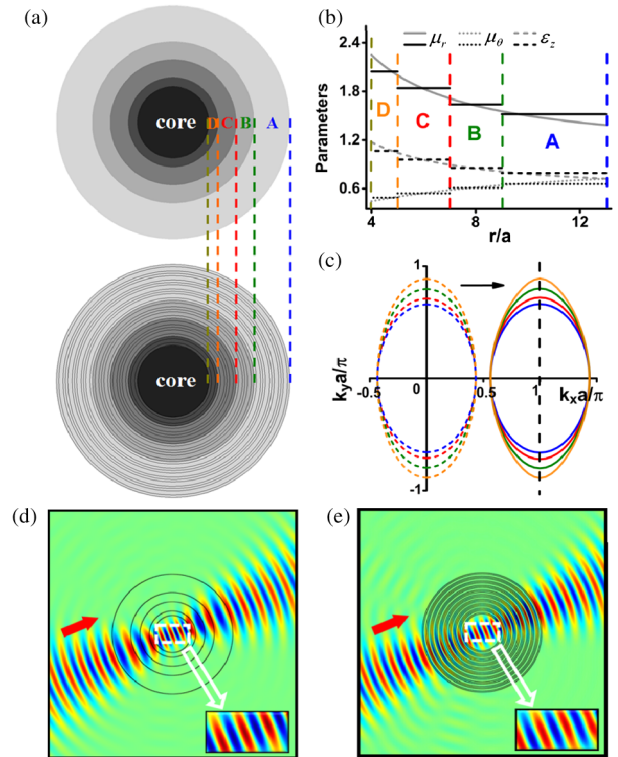

FIG. 4. (a) Illustration of the design process from a concentrator composed of discretized layers of TO media (upper) to one composed of ultratransparent 1D PhCs (lower). (b) Parameters of the discretized layers of TO media (black) and the ideal profile (grey). (c) EFCs of the discretized layers of TO media (dashed lines) and the corresponding PhCs (solid lines). Electric field distributions in (d) the concentrators made of discretized TO media, and (e) ultratransparent PhCs.

enhancement compared with that through an alumina slab with the same thickness (dashed lines). Although the ultratransparency effect is hereby only verified at the microwave frequency regime, the principle can be extended to the optical frequency regime by using microstructures composed of silicon or other dielectrics [10,11].

Finally, we demonstrate that such ultratransparent media provide an excellent platform for realizing TO devices at optical frequencies. The impedance and refractive behavior of the dielectric PhCs can be flexibly tuned to satisfy the requirement of TO. Interestingly, the shift of the EFC provides additional freedom beyond the original framework of TO [23,24] based on local media. As shown in Fig. 1(d), an additional phase of pd is added to all transmitted waves (see the Supplemental Material [47], Sec. V), where d is the thickness of the PhC slab. Therefore, the phase of the transmitted waves can be controlled via this new degree of freedom absent in local media.

As an example of TO devices, we demonstrate a concentrator composed of one-dimensional (1D) ultratransparent PhCs. The design process is shown in Fig. 4(a), in which the original shell of a concentrator [38] is discretized into four layers and each layer is further replaced by a corresponding 1D ultratransparent PhC (see the Supplemental Material [47], Sec. VII). Figure 4(b) shows the parameters of the discretized layers of TO media and the ideal profile. The corresponding four types of 1D ultratransparent PhCs are of the same lattice constant a, and of 4, 2, 2, and 1 units for the A, B, C, and D layers, respectively. The EFCs of PhCs and the discretized layers of TO media are shown in Fig. 4(c). It can be seen that the EFCs of PhCs have almost the same

shapes with their corresponding layers, but are shifted by π/a in the k space. Through numerical simulations, we demonstrate that such a concentrator composed of 1D ultratransparent PhCs exhibits almost the same effect as the original discretized TO concentrator. Figures 4(d) and 4(e) show that under an incident beam of Gaussian wave from the lower left, both concentrators exhibit good concentration effects in the core areas and induce almost no scattering of waves. Interestingly, the waves inside the core areas exhibit a distinct phase difference of π. This discrepancy is a result of the new freedom introduced by the shift of EFCs in the k space, i.e., spatial dispersion.

We note that the theory of TO has been generalized to nonlocal media [55–57], but previous realizations were mostly based on metal-dielectric composites at the deep subwavelength scale [55]. Here, we have utilized the inherent spatial dispersions in PhCs to realize TO devices, with the significant advantages of wide-angle impedance matching, low loss, and microfabrication at optical frequencies.

Although the ultratransparency effect is only demonstrated for TE polarization here, the principle is general and can be extended to transverse magnetic (TM) polarization,

or even both polarizations. Polarization-independent ultra-transparency has wide and important applications. On the other hand, polarization-dependent ultratransparent media could also have some special applications. For instance, if the PhC is ultratransparent for TE polarization, while the working frequency falls in an omnidirectional band gap for TM polarization, such a PhC would work as an omnidirectional polarizer.

The method of designing spatially dispersive effective parameters to realize wide-angle impedance matching is fundamentally different from previous approaches developed for local media such as designing suitable anisotropy. Our work shows that spatial dispersions can not only lead to exotic refractive behaviors (which is determined by EFCs of PhCs) but also produce exotic wide-angle non-reflective behavior. Here, the design principle lies in systematic tuning of the microstructures of the PhCs based on the retrieved spatially dispersive effective parameters, so as to improve the wide-angle impedance matching. More applications can be expected by utilizing the new degrees of freedoms in designing spatially dispersive effective parameters.

---

*Corresponding author.
zhhang@suda.edu.cn
†Corresponding author.
laiyun@suda.edu.cn

[1] E. Yablonovitch, Inhibited spontaneous emission in solid-state physics and electronics, Phys. Rev. Lett. **58**, 2059 (1987).

[2] S. John, Strong localization of photons in certain disordered dielectric superlattices, Phys. Rev. Lett. **58**, 2486 (1987).

[3] J. D. Joannopoulos, P. R. Villeneuve, and S. Fan, Photonic crystals: Putting a new twist on light, Nature (London) **386**, 143 (1997).

[4] J. D. Joannopoulos, S. G. Johnson, J. N. Winn, and R. D. Meade, *Photonic Crystals: Molding the Flow of Light*, 2nd ed. (Princeton University Press, Princeton, USA, 2008).

[5] K. Sakoda, *Optical Properties of Photonic Crystals* (Springer, New York, 2005).

[6] K. Ho, C. Chan, and C. Soukoulis, Existence of a photonic gap in periodic dielectric structures, Phys. Rev. Lett. **65**, 3152 (1990).

[7] A. Mekis, J. C. Chen, I. Kurland, S. H. Fan, P. R. Villeneuve, and J. D. Joannopoulos, High transmission through sharp bends in photonic crystal waveguides, Phys. Rev. Lett. **77**, 3787 (1996).

[8] S. Lin, E. Chow, V. Hietala, P. R. Villeneuve, and J. D. Joannopoulos, Experimental demonstration of guiding and bending of electromagnetic waves in a photonic crystal, Science **282**, 274 (1998).

[9] Y. Akahane, T. Asano, B. Song, and S. Noda, High-Q photonic nanocavity in a two-dimensional photonic crystal, Nature (London) **425**, 944 (2003).

[10] A. Blanco, E. Chomski, S. Grabtchak, M. Ibisate, S. John, S. W. Leonard, C. Lopez, F. Meseguer, H. Miguez, J. P. Mondia, G. A. Ozin, O. Toader, and H. M. van Driel, Large-scale synthesis of a silicon photonic crystal with a complete three-dimensional bandgap near 1.5 micrometres, Nature (London) **405**, 437 (2000).

[11] Y. A. Vlasov, X. Bo, J. C. Sturm, and D. J. Norris, On-chip natural assembly of silicon photonic bandgap crystals, Nature (London) **414**, 289 (2001).

[12] Y. Shen, D. Ye, I. Celanovic, S. G. Johnson, J. D. Joannopoulos, and M. Soljacic, Optical broadband angular selectivity, Science **343**, 1499 (2014).

[13] H. Kosaka, T. Kawashima, A. Tomita, M. Notomi, T. Tamamura, T. Sato, and S. Kawakami, Superprism phenomena in photonic crystals, Phys. Rev. B **58**, R10096 (1998).

[14] M. Notomi, Theory of light propagation in strongly modulated photonic crystals: Refractionlike behavior in the vicinity of the photonic band gap, Phys. Rev. B **62**, 10696 (2000).

[15] C. Luo, S. Johnson, J. Joannopoulos, and J. Pendry, All-angle negative refraction without negative effective index, Phys. Rev. B **65**, 201104 (2002).

[16] E. Cubukcu, K. Aydin, E. Ozbay, S. Foteinopoulou, and C. M. Soukoulis, Electromagnetic waves: Negative refraction by photonic crystals, Nature (London) **423**, 604 (2003).

[17] Y. A. Urzhumov and D. R. Smith, Transformation optics with photonic band gap media, Phys. Rev. Lett. **105**, 163901 (2010).

[18] Z. Liang and J. Li, Scaling two-dimensional photonic crystals for transformation optics, Opt. Express **19**, 16821 (2011).

[19] J. B. Pendry, A. J. Holden, W. J. Stewart, and I. I. Youngs, Extremely low frequency plasmons in metallic mesostructures, Phys. Rev. Lett. **76**, 4773 (1996).

[20] J. B. Pendry, A. J. Holden, D. J. Robbins, and W. J. Stewart, Magnetism from conductors and enhanced nonlinear phenomena, IEEE Trans. Microwave Theory Tech. **47**, 2075 (1999).

[21] D. R. Smith, J. B. Pendry, and M. C. Wiltshire, Metamaterials and negative refractive index, Science **305**, 788 (2004).

[22] Y. Liu and X. Zhang, Metamaterials: a new frontier of science and technology, Chem. Soc. Rev. **40**, 2494 (2011).

[23] J. B. Pendry, D. Schurig, and D. R. Smith, Controlling electromagnetic fields, Science **312**, 1780 (2006).

[24] U. Leonhardt, Optical conformal mapping, Science **312**, 1777 (2006).

[25] D. Schurig, J. J. Mock, B. J. Justice, S. A. Cummer, J. B. Pendry, A. F. Starr, and D. R. Smith, Metamaterial electromagnetic cloak at microwave frequencies, Science **314**, 977 (2006).

[26] W. Cai, U. K. Chettiar, A. V. Kildishev, and V. M. Shalaev, Optical cloaking with metamaterials, Nat. Photonics **1**, 224 (2007).

[27] J. Li and J. B. Pendry, Hiding under the carpet: A new strategy for cloaking, Phys. Rev. Lett. **101**, 203901 (2008).

[28] R. Liu, C. Ji, J. J. Mock, J. Y. Chin, T. J. Cui, and D. R. Smith, Broadband ground-plane cloak, Science **323**, 366 (2009).

[29] J. Valentine, J. Li, T. Zentgraf, G. Bartal, and X. Zhang, An optical cloak made of dielectrics, Nat. Mater. **8**, 568 (2009).

[30] L. H. Gabrielli, J. Cardenas, C. B. Poitras, and M. Lipson, Silicon nanostructure cloak operating at optical frequencies, Nat. Photonics **3**, 461 (2009).

[31] T. Ergin, N. Stenger, P. Brenner, J. B. Pendry, and M. Wegener, Three-dimensional invisibility cloak at optical wavelengths, Science **328**, 337 (2010).

[32] H. F. Ma and T. J. Cui, Three-dimensional broadband ground-plane cloak made of metamaterials, Nat. Commun. **1**, 21 (2010).

[33] S. Xu, X. Cheng, S. Xi, R. Zhang, H. O. Moser, Z. Shen, Y. Xu, Z. Huang, X. Zhang, F. Yu, B. Zhang, and H. Chen, Experimental demonstration of a free-space cylindrical cloak without superluminal propagation, Phys. Rev. Lett. **109**, 223903 (2012).

[34] J. Zhu, W. Jiang, Y. Liu, G. Yin, J. Yuan, S. He, and Y. Ma, Three-dimensional magnetic cloak working from d.c. to 250 kHz, Nat. Commun. **6**, 8931 (2015).

[35] N. Landy and D. R. Smith, A full-parameter unidirectional metamaterial cloak for microwaves, Nat. Mater. **12**, 25 (2013).

[36] B. Zhang and B. Wu, Electromagnetic detection of a perfect invisibility cloak, Phys. Rev. Lett. **103**, 243901 (2009).

[37] Q. Ma, Z. L. Mei, S. K. Zhu, T. Y. Jin, and T. J. Cui, Experiments on active cloaking and illusion for Laplace equation, Phys. Rev. Lett. **111**, 173901 (2013).

[38] M. Rahm, D. Schurig, D. A. Roberts, S. A. Cummer, D. R. Smith, and J. B. Pendry, Design of electromagnetic cloaks and concentrators using form-invariant coordinate transformations of Maxwell's equations, Photonics Nanostruct. Fundam. Appl. **6**, 87 (2008).

[39] Y. Lai, J. Ng, H. Chen, D. Han, J. Xiao, Z. Zhang, and C. Chan, Illusion optics: The optical transformation of an object into another object, Phys. Rev. Lett. **102**, 253902 (2009).

[40] J. Pendry, All smoke and metamaterials, Nature (London) **460**, 579 (2009).

[41] D. A. Genov, S. Zhang, and X. Zhang, Mimicking celestial mechanics in metamaterials, Nat. Phys. **5**, 687 (2009).

[42] C. Sheng, H. Liu, Y. Wang, S. N. Zhu, and D. A. Genov, Trapping light by mimicking gravitational lensing, Nat. Photonics **7**, 902 (2013).

[43] R. Bekenstein, R. Schley, M. Mutzafi, C. Rotschild, and M. Segev, Optical simulations of gravitational effects in the Newton–Schrödinger system, Nat. Phys. **11**, 872 (2015).

[44] C. Sheng, R. Bekenstein, H. Liu, S. Zhu, and M. Segev, Wavefront shaping through emulated curved space in waveguide settings, Nat. Commun. **7**, 10747 (2016).

[45] S. Xiao, V. P. Drachev, A. V. Kildishev, X. Ni, U. K. Chettiar, H. K. Yuan, and V. M. Shalaev, Loss-free and active optical negative-index metamaterials, Nature (London) **466**, 735 (2010).

[46] O. Hess, J. B. Pendry, S. A. Maier, R. F. Oulton, J. M. Hamm, and K. L. Tsakmakidis, Active nanoplasmonic metamaterials, Nat. Mater. **11**, 573 (2012).

[47] See Supplemental Material at http://link.aps.org/supplemental/10.1103/PhysRevLett.117.223901, for details of derivations and analysis of omnidirectional impedance matching, aberration-free virtual imaging, effective parameters, dependence of transmission on lattice constants, additional freedom in controlling phases, experimental PhCs and 1D PhCs, which includes Refs. [48–51].

[48] W. Śmigaj and B. Gralak, Validity of the effective-medium approximation of photonic crystals, Phys. Rev. B **77**, 235445 (2008).

[49] Z. Lu and D. W. Prather, Calculation of effective permittivity, permeability, and surface impedance of negative-refraction photonic crystals, Opt. Express **15**, 8340 (2007).

[50] F. J. Lawrence, C. M. de Sterke, L. C. Botten, R. C. McPhedran, and K. B. Dossou, Modeling photonic crystal interfaces and stacks: impedance-based approaches, Adv. Opt. Photonics **5**, 385 (2013).

[51] D. R. Smith and J. B. Pendry, Homogenization of metamaterials by field averaging, J. Opt. Soc. Am. B **23**, 391 (2006).

[52] F. Aieta, P. Genevet, M. A. Kats, N. Yu, R. Blanchard, Z. Gaburro, and F. Capasso, Aberration-free ultrathin flat lenses and axicons at telecom wavelengths based on plasmonic metasurfaces, Nano Lett. **12**, 4932 (2012).

[53] F. Monticone, C. A. Valagiannopoulos, and A. Alù, Parity-Time Symmetric Nonlocal Metasurfaces: All-Angle Negative Refraction and Volumetric Imaging, Phys. Rev. X **6**, 041018 (2016).

[54] X. D. Zhang, Z. Q. Zhang, L. M. Li, C. Jin, D. Zhang, B. Man, and B. Cheng, Enlarging a photonic band gap by using insertion, Phys. Rev. B **61**, 1892 (2000).

[55] G. Castaldi, V. Galdi, A. Alù, and N. Engheta, Nonlocal transformation optics, Phys. Rev. Lett. **108**, 063902 (2012).

[56] A. I. Fernández-Domínguez, A. Wiener, F. J. García-Vidal, S. A. Maier, and J. B. Pendry, Transformation-optics description of nonlocal effects in plasmonic nanostructures, Phys. Rev. Lett. **108**, 106802 (2012).

[57] Y. Luo, A. I. Fernandez-Dominguez, A. Wiener, S. A. Maier, and J. B. Pendry, Surface plasmons and nonlocality: A simple model, Phys. Rev. Lett. **111**, 093901 (2013).